

Numerical experiments on the generation of normal mode Rossby waves

Hyeong-Bin Cheong and In-Hyuk Kwon

Dept. of Atmospheric Sciences, Pukyong National University
(599-1 Daeyeon-3-dong, Namgu, Busan 608-737, Korea)

Abstracts

Normal mode Rossby waves are simulated with an efficient Double Fourier Series (DFS) spectral model, and their structures are investigated by the Empirical Orthogonal Function (EOF) analysis. By selecting appropriately the wave-vector component for EOF analysis among the geopotential height and velocity fields of wavenumber one, it was possible to get the EOFs from the time series data whose spatial structures closely resemble the gravest three normal-mode waves. It was found that the leading modes of EOFs showed the phase configuration that tilts northward-westward and upward-westward in the horizontal and vertical plane, respectively. This indicates, as in the previous studies, that the normal mode Rossby waves are generated by the wave source in the lower atmosphere of southern-hemisphere high-latitudes. The wave amplitude of the temperature field that was obtained from the hydrostatic equation was shown to increase with the altitude except the upper tropospheric layers.

Keywords: Rossby normal mode waves, double Fourier series, empirical orthogonal function, wave source, phase tilt, time filtering

1. Introduction

Normal mode global Rossby waves are the westward-propagating free oscillations of the global atmosphere at rest subject to the gravity and Coriolis force, whose horizontal structures are given by Hough functions (Longuet-Higgins 1968; Kasahara 1980; Salby 1984; Daley 1991). Since the theoretical prediction of these normal mode waves, they have been detected in the atmosphere by many authors using sophisticated statistical methods (Madden and Julian 1972; Lindzen et al. 1984; Salby 1984; Ahlquist 1985; Hirooka and Hirota 1985; Randel 1993; Cheong and Kimura 1997, 2001; Cheong and Kwon 2003). The amplitudes of the normal modes are usually so small that they are not easily seen in the weather charts, but their impact on the atmospheric general circulation seems to be quite significant (e.g., Hirooka 1986; Randel 1993; Lejenäs and Madden 2000). Of the normal modes, the 5-day-, 10-day- and 16-day waves, which are the observational counterpart of the Hough modes H_1^1 , H_2^1 and H_3^1 [super- and

sub-script denote the zonal wavenumber and the meridional wavenumber-like index (nodal points)], respectively, are of particular interest; They are little affected by the presence of the zonal-mean flow due to large frequency and meridional scale (Kasahara 1980; Salby 1981).

In this paper, the normal modes waves are simulated using an efficient DFS spectral model, and their structures are investigated in terms of Empirical Orthogonal Function (EOF) analysis. Unlike other methods used in previous studies for the normal mode analysis, EOF method provides three-dimensional empirical modes of disturbances either traveling or stationary which are orthogonal one another (cf. Brunet and Vautard 1996). The EOF analysis is focused on the normal modes of H_1^1 , H_2^1 and H_3^1 by filtering the zonal wavenumber-one data with appropriate bandpass filters.

2. Numerical model and analysis Method

The numerical model used in this study is an efficient DFS model (Cheong 2006). The model parameters are the same as in Cheong (2006) but with T42 horizontal resolution (horizontal gridpoints of 144×72). The simulation is carried out for 1400 days, and the last 1200 data are analyzed. Analyzed variables are geopotential height, and zonal and meridional velocities of 6 pressure levels of 850, 500, 200, 100, 50 and 20 hPa (i.e., total of 18 variables: $Z_{850}, \dots, Z_{20}, U_{850}, \dots, U_{20}, V_{850}, \dots, V_{20}$) with one day interval. For convenience, the time-series data set is denoted by four dimensional array $X(i, j, k, t)$, where i ($=1, \dots, 144$) and j ($=1, \dots, 73$) are zonal and meridional index, respectively, and k ($=1, \dots, 6$) and t are for the vertical and time-series index, respectively. The procedure of data analysis is the same as in Cheong and Kwon (2003), where 61 points bandpass-filters were used to choose westward traveling disturbances associated with a Hough mode (Hayashi 1971; Hamming 1977).

3. Results

The EOF analysis was performed for the summer season (from 15 APR to 14 OCT) and winter (from 15 OCT to 14 APR) separately, because the activities of the normal modes have a large seasonal variation (Lindzen et al. 1984; Ahlquist 1985; Cheong and Kimura 1997, 2001). From the eigenvalues-eigenvectors analysis it was found that two neighboring modes (e.g., a mode with odd number and following even-number mode) have the same eigenvalue, of which the first pair explains more than 50 % of the total variance included in the time-filtered data and the contribution of the second pair drops sharply to less than a half of the first pair. The leading modes are identified as the gravest modes for each time filtered data as in Cheong and Kwon (2003).

In Fig. 1 the spatial structure of the leading mode is presented for three cases in terms of the geopotential height and the velocity vectors at 850 hPa level. The second mode is identical to the first mode but with the zonal phase-lag of a quarter cycle (not shown). By projecting the EOFs to the time-filtered data to get the time-series (Brunet and Vautard 1996; Golub and Van Loan 1996), it was shown

that both the first and second mode exhibit time fluctuation with almost the same frequency but with a phase-lead of the second mode by a quarter cycle over the first mode. This means that a pair of modes with the same eigenvalue represents a westward traveling wave as will be shown below in terms of the phase diagram (Fig. 2). This wave can be expressed by $A_{1,2}(t)F_{1,2}(\lambda, \theta)$ where $A_{1,2}(t) \left[\equiv \sqrt{A_1(t)^2 + A_2(t)^2} \right]$ is the time series and $F_{1,2} \left[\equiv B(\theta) \cos(\lambda + \omega t + \Xi) \right]$ is the spatial pattern with λ being the longitude, ω the frequency, $B(\theta)$ the meridional function and $\Xi(\theta)$ the zonal-phase. The frequency ω is not constant, but varies slowly with time around the mean frequency $\bar{\omega}$.

Note that the first EOF mode of FLTR1 (time filtered with 3-7 days bandpass filter) is very close to the 5-day wave detected by a composite method from the 7-years ECMWF dataset, which is characterized by the SE-NW phase tilt and larger amplitude being found in the high latitude of the southern hemisphere (Cheong and Kimura 1997). The velocity vectors closely follow the geopotential height contour lines except the equatorial region, indicating the quasi-geostrophic balance (Longuet Higgins 1968; Salby 1984; Daley 1991). The structures of the modes for FLTR2 (6-14 days bandpass filtered data) and FLTR3 (10-10 days bandpass filter) are also similar to 10-day and 16-day waves, respectively, presented in Cheong and Kimura (2001) except that the eigenmode for FLTR2-winter has smoother zonal-phase variation with the latitude and larger hemispheric asymmetry compared with Cheong and Kimura (2001). From the horizontal structures in Fig. 1 and the vertical variation of the amplitudes that will be shown in Fig. 3, the first pairs of modes of FLTR1, FLTR2 and FLTR3 may be referred to as 5-day, 10-day and 16-day wave, respectively.

For each time-filtered dataset, the structures of the EOF modes other than the first pair are found be far from those of the observed normal modes such as 5-day, 10-day and 16-day waves. If the composite analysis method in Cheong and Kimura (1997, 2001) is applied to the time-filtered data produced in the second step described in the previous section, the composite map might resemble the first modes shown in Fig. 1. This is because the EOF modes are independent one another and the mode with a low relative-contribution will disappear in the composite procedure leaving only a dominant mode (cf. Madden and Julian 1972).

The mean periods ($2\pi\bar{\omega}$) of the first pair of modes are about 4.86, 9.9 and 14.8 day for FLTR1, FLTR2 and FLTR3, respectively, which are quite close to the period of the 5-day, 10-day and 16-day waves observed in the atmosphere (Madden and Julian 1972; Madden 1978; Hirooka and Hirota 1985; Cheong and Kimura 1997, 2001). The mean amplitude of the first pair of EOF modes, defined by

$$\langle A_{1,2}(t) \rangle = \left[\frac{1}{P} \sum_{t=1}^P A_{1,2}(t)^2 \right]^{1/2} \text{ with } P \text{ being the number of maps corresponding to 40-year period,}$$

is 23.79 (18.57) for FLTR1-summer (winter) season. The mean amplitudes for FLTR2-summer (winter) and FLTR3-summer (winter) are 43.82 (28.76) and 55.56 (33.90), respectively. The geopotential-height disturbance associated with the first pair of modes is then calculated by multiplying the mean amplitude to the EOFs in Fig. 1, which gives about 12, 21 and 22 gpm at 850 hPa level for FLTR1, FLTR2 and FLTR3, respectively.

Fig. 3 shows the vertical amplitude variation of the EOF modes shown in Fig. 1 and the layer-mean temperature calculated from the hydrostatic-balance equation, $\frac{\partial \Phi}{\partial \ln p} = -RT$ where Φ , p , R

and T are the geopotential, pressure, gas constant and temperature, respectively. The amplitude of geopotential height increases with a small slope for the FLTR1 but with fairly large slopes for the FLTR2 and FLTR3. In either case, the amplitude increases more sharply than is predicted by the exponential function of the log-pressure (Salby 1984; Daley 1991; Cheong and Kimura 1997). The temperature varies little in the lower layers, but also shows a steep increase with height. Interestingly, the amplitude of the temperature decreases with height around the tropopause for all modes except FLTR1-summer season. Maximum amplitudes of layer-mean temperature are found between 50 hPa and 20 hPa level, whose 40-year averages are about 0.23 K, 0.86 K and 1.30 K for the 5-day, 10-day and 16-day waves. The amplitude of the waves in Fig. 1 [that is, the time-series $A_{1,2}(t)$] undergoes a considerable year-to-year variation. The year-mean maximum amplitude of the 16-day waves appear in the summer season of 1987 with $\langle A_{1,2}(t) \rangle_{1987} = 77.8$, where the amplitude of the temperature disturbance averaged between 50hPa and 20hPa level becomes approximately 2 K.

The EOF modes in Fig. 1 have vertical phase tilt of westward-upward (not shown), which is about 30 degrees between the 850 hPa and 20 hPa level. Together with the NW-SE horizontal phase tilt as shown in Fig 1, this phase configuration suggests that the wave source exists in the high-latitudes of the southern hemisphere except the 16-day waves in winter season (Garcia and Salby 1987; Manzini and Hamilton 1993; Cheong and Kimura 1997, 2001).

4. Discussion and Conclusions

Normal mode Rossby waves of zonal wavenumber-one were simulated using DFS spectral model, and analyzed by EOF analysis with a focus on the three largest Hough modes. A pair of EOF modes of the 3-7 day time-filtered data with the largest variance was identified as the 5-day wave, while those of 6-14 days (10-20 days) were identified as the 10-day (16-day) wave. They share many common features with those detected from NCEP-NCAR and ECMWF dataset by the composite method. The amplitude of the 5-day waves was comparable to that found in the previous studies, but the amplitudes of the 10-day and 16-day waves were larger.

The amplitude of the temperature disturbance associated with the three EOF modes was found to be significantly small, reaching at most 0.02 K and 0.1 K for the 5-day and 16-day waves, respectively. The amplitude of the disturbances associated with the EOF modes increases with height, of which slope is much larger than those of the previous studies. The amplitude of the temperature, however, unlike the height and velocities disturbances, decreases slightly around the tropopause, which is common to the three modes of interest in this study. The results of this study support the linear theory and observational analysis of Cheong and Kimura (1997, 2001) on the excitation mechanism.

References

- Ahlquist, J., 1985: Climatology of normal mode Rossby waves. *J. Atmos. Sci.*, 42, 2059-2068.
- Brunet, G., and R. Vautard, 1996: Empirical normal mode versus empirical orthogonal functions for statistical prediction. *J. Atmos. Sci.*, 53, 3468-3489.
- Cheong, H.-B., and R. Kimura, 1997: Excitation of the 5-day wave by Antarctica. *J. Atmos. Sci.*, 54, 87-102.
- Cheong, H.-B., and R. Kimura, 2001: Excitation of the 10-day and 16-day waves. *J. Atmos. Sci.*, 58, 1129-1145.
- Cheong, H.-B., and I.-H. Kwon, 2003: EOF analysis of the normal mode Rossby waves. *J. Kor. Meteor. Soc.*, 39, 607-619.
- Cheong, H.-B., 2006: A dynamical core with double Fourier series: Comparison with spherical harmonics method. *Mon. Wea. Rev.*, 134, 1299-1315.
- Daley, R., 1991: *Atmospheric data analysis*, Cambridge University Press, 457pp.
- Garcia, R., and M. Salby, 1987: Transient response to localized episodic heating in the tropics. Part II: Far field behavior. *J. Atmos. Sci.*, 44, 499-530.
- Golub, G. H., and C. F. Van Loan, 1996: *Matrix computations* (3rd ed.). John Hopkins University Press, 476pp.
- Hamming, R. W., 1977: *Digital filters*. Prentice-Hall, 230pp.
- Hayashi, Y., 1971: A generalized method of resolving disturbances into progressive and retrogressive waves by space Fourier and time cross-spectral analyses. *J. Meteor. Soc. Japan*, 49, 125-128.
- Hirooka, T., and I. Hirota, 1985: Normal mode Rossby waves observed in the upper stratosphere. Part II: Second antisymmetric and symmetric modes of zonal wavenumbers 1 and 2. *J. Atmos. Sci.*, 42, 536-548.
- Hirooka, T., 1986: Influence of normal mode Rossby waves on the mean field: Interference with quasi-stationary waves. *J. Atmos. Sci.*, 43, 2088-2097.
- Kasahara, A., 1980: Effect of zonal flows on the free oscillations of a barotropic atmosphere. *J. Atmos. Sci.*, 37, 917-929. Kasahara, A., and J.-H. Qian, 2000: Normal-modes of a global nonhydrostatic atmospheric model. *Mon. Wea. Rev.*, 128, 3357-3375.

Lejenäs, H., and R. A. Madden, 2000: Mountain torques caused by normal-mode global Rossby waves, and the impact on atmospheric angular momentum. *J. Atmos. Sci.*, **57**, 1045–1051.

Lindzen, R. S., D. M. Straus and B. Katz, 1984: An observational study of large scale atmospheric Rossby waves during FGGE. *J. Atmos. Sci.*, **41**, 1320-1335.

Madden, R., and P. Julian, 1972: Further evidence of global-scale, 5-day pressure wave. *J. Atmos. Sci.*, **29**, 1464-1469.

Manzini, E., and K. Hamilton, 1993: Middle atmospheric traveling waves forced by latent and convective heating. *J. Atmos. Sci.*, **50**, 2180-2200.

Randel, W. J., 1993: Global normal mode Rossby waves observed in stratospheric ozone data. *J. Atmos. Sci.*, **50**, 406-420.

Salby, M., 1981: Rossby normal modes in nonuniform background configurations. Part I: Simple fields. *J. Atmos. Sci.*, **38**, 1803-1826.

Salby, M., 1984: Survey of planetary-scale traveling waves: The state of theory and observations. *Rev. Geophys. Space Phys.*, **22**, 209-236.

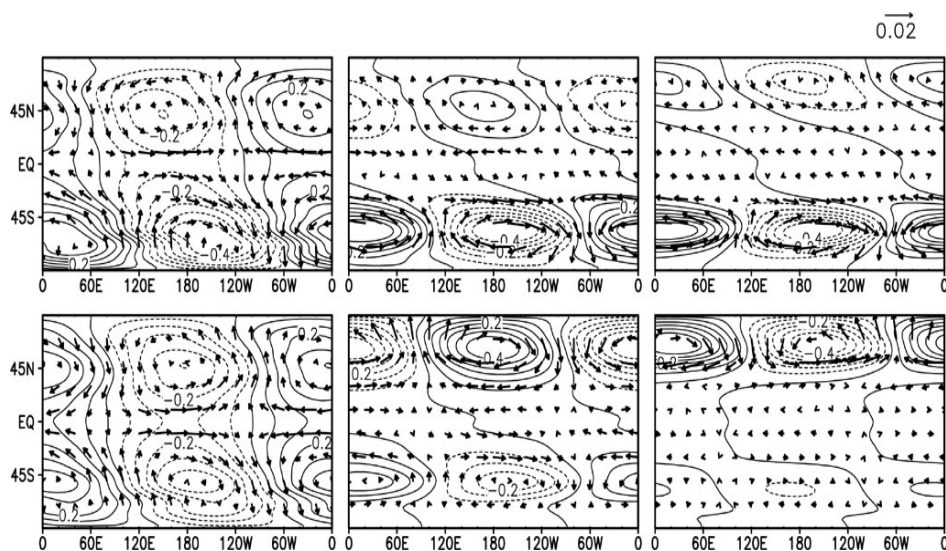


Figure 1 Geopotential height (contour lines) and velocity vectors (arrows) at 850 hPa level of the first EOF modes obtained from time filtered data of 3-7 days (left column), 8-14 days (middle) and 10-20 days (right), respectively. Maps in the upper (lower) row are for the summer (winter) season. The contour interval is 0.0667 and the negative values are drawn with dashed lines.

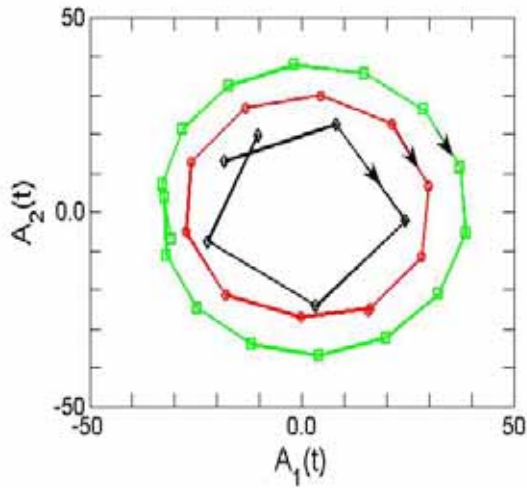


Figure 2 Plot of time-series of the first $[A_1(t)]$ and the second mode $[A_2(t)]$ for about one cycle taken from the summer season of 1988, where the black (from day 39 to 44), red (from day 2 to 11) and green (from day 82 to 97) lines represent the EOF modes of the FLTR1, FLTR2 and FLTR3, respectively. The arrow indicates the direction of time increase and the anticlockwise rotation means the westward propagation of the EOF mode.

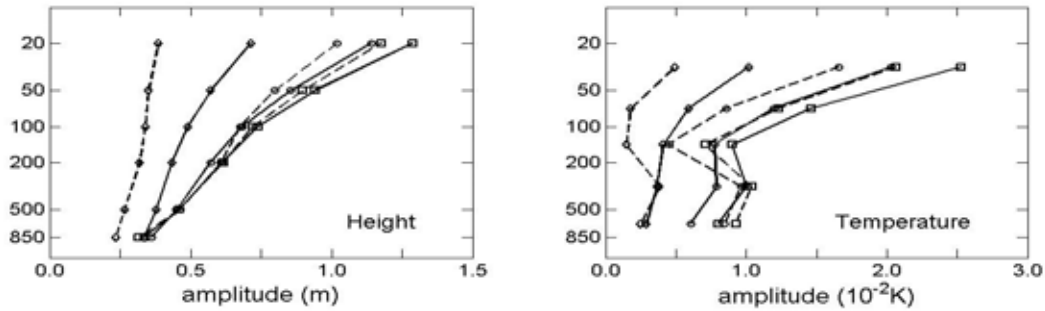


Figure 3 (Left) Vertical amplitude variation of the EOF modes shown in Fig. 1, where the solid (dashed) lines are for the summer (winter). Diamond marks, circles and squares represent the FLTR1, FLTR2 and FLTR3, respectively. (Right) Same as the left panel but the amplitude of the temperature averaged between two pressure levels. The amplitude was calculated at 60S except for the winter seasons of FLTR2 and FLTR3 for which 60N was used (see Fig. 1). The observed mean-amplitude of the modes should be multiplied by the mean-amplitude of the time series (e.g., multiplication factor of 55.56 for FLTR3-summer; see the text for details).

Acknowledgements

This work was supported by PuKyong National University Research Foundation Grant in 2005 (PR-2005-007).